50th AIAA Aerospace Sciences Meeting
9 - 12 Jan 2012, Nashville, TN
AIAA-2012-0623

The Study of Aero-Optical and Mechanical Jitter for Flat Window Turrets

Nicholas De Lucca[1], Stanislav Gordeyev[2], and Eric Jumper[3]
University of Notre Dame, Notre Dame, Indiana, 46545

Simultaneous local jitter, 2-D wavefronts and accelerometer measurements were performed in the flow over a flat-window turret at Mach numbers between 0.3 and 0.4 along a centerplane with a viewing angle varying between 90 and 118 degrees. Both local and global jitter imposed on a small- and large-aperture laser beams were measured using position-sensing devices and a high-speed 2-D wavefront sensor. A linear stochastic estimation technique was applied to separate the mechanically-related component of the jitter from the aero-optical component. Spectra of aero-optical jitter for different elevation angles and speeds were calculated and useful scaling laws were proposed. It was shown that aero-optical jitter was due to the presence of both the stationary and traveling aero-optical components. Detailed analysis of the global and the local jitter spectra and the spectral cross-correlation between them at different speeds and viewing angles is presented and discussed in details. Additionally, PIV system was used to measure the flow field over the flat window, simultaneously with the aero-optical jitter measurements.

I. Introduction

FOR optical considerations, hemisphere-on-cylinder turrets are excellent platforms for laser applications, due to large fields of view; however, when placed upon a moving body at subsonic or greater speeds, they create very complex flow fields [1]. At these speeds, the flow field induces significant unsteady density fluctuations around turrets which create large spatially- and temporally-varying aberrations in laser beams propagating through them. This is traditionally referred to as the aero-optical problem [2]. The density of the fluid can be related to its index of refraction through the Gladstone-Dale constant, $n(x,y,z,t)-1=K_{GD}\rho(x,y,z,t)$. As the index of refraction varies in both space and time, an incident planar wavefront on the flow is distorted. The aberrations induced in the wavefront arise from parts of the wavefront travelling different distances in a given time period due to the spatial variance in the index of refraction. Knowing the index-of-refraction field, the optical path length, *OPL*, can be found using $OPL(x,y,t)=\int_{s1}^{s2} n(x,y,z,t)ds$. The measured deviation of the wavefront from its initial planar form, the optical path difference, *OPD*, can be computed from the *OPL* as $OPD(x,y,t)=OPL(x,y,t)-\overline{OPL(x,y,t)}$, where the overbar denotes the spatial averaging. Note that the wavefront is just a negative or conjugate of the *OPD*, $W(x,y,t) = - OPD(x,y,t)$. Through the computation of various statistics of the *OPD*, such as the mean spatial RMS or the temporal RMS, the quality of a measured wavefront can be characterized.

The hemisphere-on-cylinder turret geometry creates several distinct flow features that combine into a highly three-dimensional flow field. The flow over the upstream portion of a turret is relatively well-behaved; it is dominated by an attached boundary layer and it has low turbulence levels compared to the rest of the flow. Near the base of the turret, a necklace vortex forms. The flow separates on top of the turret with the separation point having a Reynolds Number dependence and a wake is formed aft of the turret. Specifically for a flat-window turret, as it was shown in [3], the slope discontinuity around the flat window creates the local separation bubble, which induces additional aero-optical aberrations over a range of the elevation angles.

---

[1] Graduate Student, Department of Mechanical and Aerospace Engineering, Hessert Laboratory for Aerospace Research, Notre Dame, IN 46556, Student Member.
[2] Research Associate Professor, Department of Mechanical and Aerospace Engineering, Hessert Laboratory for Aerospace Research, Notre Dame, IN 46556, Senior AIAA Member.
[3] Professor, Department of Mechanical and Aerospace Engineering, Hessert Laboratory for Aerospace Research, Notre Dame, IN 46556, AIAA Fellow.

It has been shown that the flow around turrets not only exhibits significant amount of high-order aero-optical distortions at back-looking angles, but also causes the laser beam to tip/tilt or jitter, so-called aero-optical jitter. In addition, the jitter has a significant mechanically-induced component due to turret elastic response to unsteady forces imposed by the flow [4], the mechanical jitter. The mechanical jitter of turrets, especially with flat-window apertures has been largely ignored in aero-optical studies, although it can significantly corrupt the ability of the beam to focus on a target and deteriorate the performance of the turret-based laser system. Due to inertia of the turret, the mechanical component is usually present at lower frequency ranges, less than half a kHz, while aero-optical distortions typically dominate at higher frequencies 1 kHz and above. The ultimate goal is not only to separate the two components for independent analysis, but to understand and be able to model each component. This includes understanding of the physical mechanisms driving each component of the jitter and how they scale with flow variables and geometry changes.

In this paper the aero-optical environment around the flat-window turret is investigated at a range of back-looking angles for subsonic speeds. In addition of measuring temporal-spatial evolution of wavefronts at different angles and speeds, the simultaneous measurements of the global jitter imposed on the large-aperture beam, as well as the local jitter of the small-aperture beam were preformed. Also, limited velocity measurements were taken over the aperture to investigate the topology of the flow field. The experimental set-up is presented in Section II with the data reduction procedures described in Section III. Results are discussed in details in Section IV and conclusions are presented in Section V.

II. Experimental Setup

Experiments are conducted with a hemisphere-on-cylinder turret with a flat window. The tests were conducted in the White Field test facility at the University of Notre Dame. The tunnel is a 3 ft. by 3 ft. subsonic closed return tunnel. The turret has 1 ft. diameter hemisphere top with a flat mirror 4-inch in diameter seated on a 6-inch tall cylindrical base; the hemispherical portion of the turret with the flat window can be rotated to any elevation angle between 70°and 118° and the turret assembly can be rotated to any azimuthal angle, see Figure 1, left. The turret was mounted on the side wall of the test section halfway between the top and the bottom walls. Accelerometers were placed on the back side of the flat window to measure the mechanical motion of the turret.

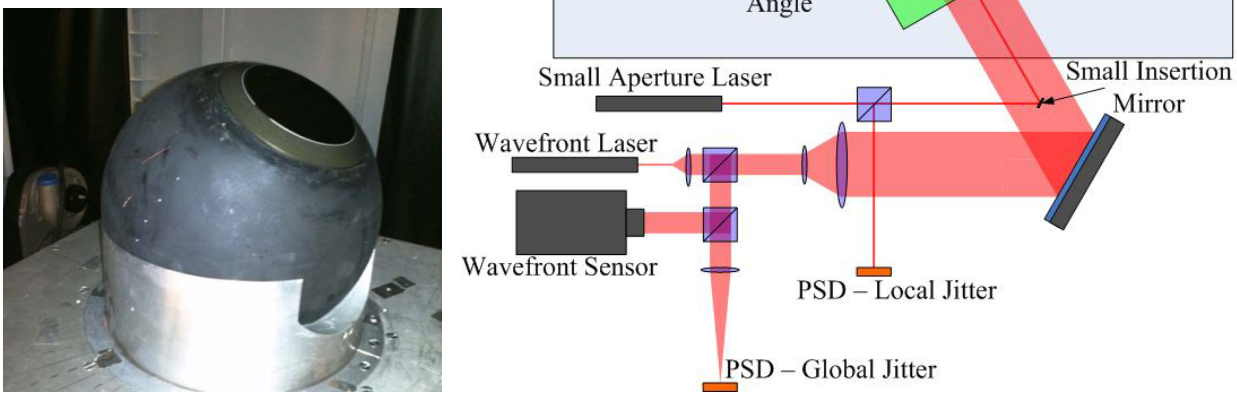

Figure 1: Left: The turret assembly. Right: The schematic of the experimental setup.

One laser beam was expanded to a 4-inch collimated beam, while the second beam was left unexpanded. Both laser beams were forwarded into the test section and were reflected normally from a flat mirror on the turret, returning back to the optical table exactly along the same path they came into the test section, so-called a double-pass set-up, see Figure 1, right. The small-aperture beam set-up was very similar to a typical Malley Probe setup [5], but only one beam was used in this experiment. The small-aperture beam was injected slightly upstream of the

center of the flat-mirror aperture using a small mirror, to minimize the obscuration, as shown in Figure 1, right. Local jitter of the small-aperture beam reflected off the flat window was measured using a Position Sensing Device (PSD), while the global jitter and higher-order wavefronts imposed on the 4-inch collimated beam were measured using a second PSD and the high-speed wavefront sensor. The wavefront sensor was a Shack-Hartmann-type sensor with a 33 x 33 lenslet array. Wavefronts were taken at 25 kHz for 0.85 seconds. Four accelerometers were placed on the back of the flat mirror, in a non-collinear fashion such that both translational and rotational motions of the turret were measured. Accelerometer and local jitter data were collected simultaneously at 100 kHz for 15 seconds. Both the wavefront sensor and the local-jitter/accelerometers system were triggered to start collecting data at the same time to ensure that they observed the same flow conditions.

A 10 kHz LaVision PIV system was used to measure the velocity field over the flat window turret. IPIV interrogation region was centered directly over the optical window with the approximate location of the PIV plane shown in Figure 1, right. The flow was seeded using a thin airfoil upstream of the turret. PIV data was acquired at 1 kHz for 5 seconds. Additional optical data were acquired simultaneously with each PIV data set by providing a common trigger to the PIV system and the 2D Wavefront system, although no results will be presented here.

The flat aperture introduces a slope discontinuity and the observed flow characteristics are dependent on the aperture viewing direction. Typically, the viewing direction of a turret is defined with an azimuthal angle and an elevation angle that can vary between 0° and 180° and 0° and 90°, respectively. All data for this paper were taken along the centerline of the turret, and as a result a more convenient viewing-angle system is used. Viewing angles ranging from 90° to 118° that would correspond to an azimuthal angle of 180° and an elevation angle of 90° to 62°. The viewing angle is defined in Figure 1, right. Finally, the smile for the turret shown in Figure 1 was filled in for all of the data presented, and as such it did not affect the flow conditions.

III. Data Reduction

Wavefront data reduction

For every measured viewing angle and Mach number, a steady component, time-dependent tip/tilt and piston were removed from each wavefront. The removed tip/tilt was not analyzed, as the global jitter was measured directly using a PSD. To analyze the instantaneous magnitude of the spatial variation in each wavefront, the $OPD_{RMS}(t)$ was computed by taking the spatial RMS of the wavefront. The $OPD_{RMS}(t)$ is an instantaneous value for the quality of a measured wavefront compared to a planar one; smaller values indicate that an individual wavefront doesn't have large wavefront variances across it and thus it is less aberrated. The temporal mean of this value, $\overline{OPD_{RMS}}$, later in this paper called OPDrms for simplicity, gives the time-averaged amount of aero-optical distortions over the aperture. As wavefronts are functions of time and space, temporal variance of wavefronts for all spatial points over the aperture was also calculated. Again, for simplicity, in this paper it will be called as the spatial distribution of OPDrms. Both OPDrms and the spatial distribution of OPDrms provide important statistics about aero-optical distortions over the aperture.

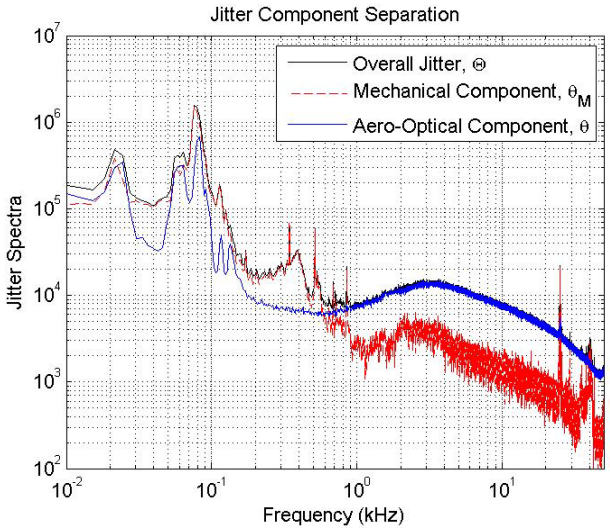

Figure 2: Example of jitter spectrum separation using LSE technique.

Jitter Reduction

To separate the mechanical and aero-optical jitter components, the linear stochastic estimation (LSE) technique was employed. This technique generates an estimate of a measured quantity using a set of other measured quantities. It does this using the correlation between a quantity to be estimated and the additional measured quantities through the cross correlation tensor of the additional quantities. The technique was developed by Adrian [6], and it can be written as $\tilde{x}_i = L_{ij} y_j$, where $L_{ij} = \langle x_i y_k \rangle \langle y_j y_k \rangle^{-1}$. Here, a measured signal, x_i, is approximated using a linear sum of other measurements, y_i, multiplied by the estimation coefficient matrix, L_{ij}. The coefficients are determined from the correlations between the signals as given by the L_{ij}-matrix. For this experiment, LSE technique was applied in the Fourier domain, so the estimation matrix, L_{ij},

becomes a function of frequency. This method has several significant advantages. It makes no assumption about the relationship between the measured quantities; it only utilizes the statistical correlation between them. The coefficients of the estimation matrix automatically account for any dimensional differences between the measured quantities (to the point of accounting for calibration coefficients automatically). Finally, the estimation matrix only needs to be solved once, making the LSE technique computationally-effective.

This technique was used to generate an estimation of the mechanically-induced part of the jitter data, both local and global, using a linear sum of the accelerometer data which was then subtracted from the original signal. Figure 2 shows the example of the LSE-based technique. Using the technique, the jitter spectra were split into the two different components. The measured overall jitter spectra, $\hat{\Theta}(f)$, consists of both the mechanically-induced jitter component, $\hat{\theta}_M(f)$, and the aero-optical component, $\hat{\theta}(f)$. The LSE reconstruction approximates the mechanically-induced component, $\theta_M \approx \tilde{x}_i$ by cross-correlating the accelerometers' spectra to the overall jitter and the aero-optical component was estimated as $\theta = \Theta - \theta_M \approx \Theta - \tilde{x}_i$. At frequencies above 600 Hz, the correlation with the mechanically induced jitter spectrum falls off very rapidly and aero-optical effects dominate at higher frequencies. Below 100 Hz, the largest contributors are from non-aero-optical effects. These include the vibration of the optical table or optical components such as mirrors and lenses and the vibration of the tunnel windows.

Power spectra for both the global and the local spectra were calculated for all measured angles and Mach numbers. Also, the spectral correlation between the global, $A(t)$, and local, $\theta(t)$, jitter was calculated using the normalized spectral correlation, $S(f) = \left\langle \hat{A}(f)\hat{\Theta}^*(f) \right\rangle \Big/ \sqrt{\left\langle \hat{A}(f)\hat{A}^*(f) \right\rangle \left\langle \hat{\Theta}(f)\hat{\Theta}^*(f) \right\rangle}$, where angled brackets denote ensemble-averaging. The magnitude of the correlation, $|S|$, gives the relative strength of the correlation between the two jitter signals at a given frequency. Taking the argument of $S(f)$ gives the phase difference between the two signals.

IV. Results

Aero-optical distortions at different viewing angles

Wavefronts for all angles and speeds were processed as described before and time-averaged spatial root-mean-squares of the tip/tilt-removed wavefronts, OPDrms, are plotted in Figure 3. OPDrms were normalized by $(\rho/\rho_{SL})M^2D$, as it was shown to be a correct scaling for aero-optical distortions around turrets at subsonic speeds [1]. Here ρ_{SL} is the sea-level density and D is the turret diameter. At M = 0.3 OPDrms have a drop around 95 degrees, then increase for higher viewing angles. For M = 0.4 values of OPDrms have a peak around 100 degrees, although not as pronounced as for M = 0.3 case. This peak in OPDrms had been observed in other experiments around both 2-D [3] and 3-D turrets [7] and had been contributed to tip/tilt aperture effects [3]. The location of the OPDrms peak was found to be a weak function of Reynolds number, most probably due to transient effects in the boundary layer on top of the turret at low speeds before it separates over the flat-window aperture.

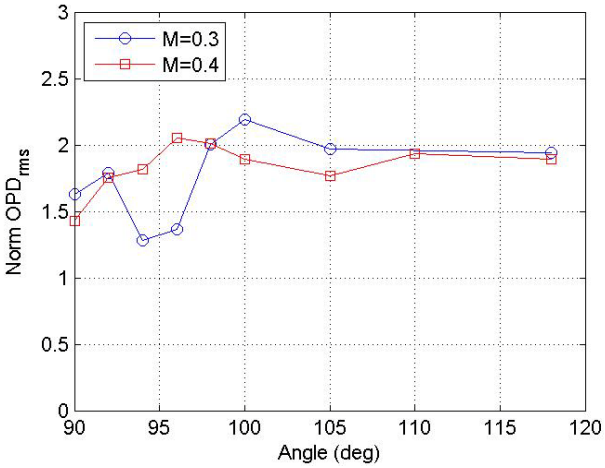

Figure 3: Overall OPDrms normalized by $(\rho/\rho_{SL})M^2D$ for M =0.3 and 0.4.

Velocity measurements over the aperture

When investigating aero-optical distortions around the 2-dimensional turret for back-looking angles [3] it was proposed that at modest back-looking viewing angles between 90 and 100 degrees a small separation bubble is formed right downstream of the slope discontinuity between the turret and the flat-window. At viewing angles larger than 100 degrees, the local separation bubble becomes an open separation region forming a shear layer over the flat-window aperture. To investigate whether a similar flow topology exists over the flat-windowed aperture for 3-D turret, PIV data were taken along the centerplane at two viewing angles, 90° and 118°, as shown in Figure 4. At the angle 90°, a small separation bubble was indeed observed at the upstream portion of the turret aperture. This bubble

is rather small, less than an inch in length, therefore it was not directly observed in the wavefronts or the local jitter measurements taken at this angle. After the separation bubble the flow re-attached and formed a boundary layer. At the angle of 118°, the separation bubble became an open separation region with a shear layer originating at the leading slope discontinuity of the flat window. The shear layer was formed when the faster free-stream flow met the recirculating flow that lies directly over the mirror. Figure 5 gives the evolution of the velocity profiles at different streamwise locations. These observed profiles match up very well with velocity profiles measured over 2-D turret [3].

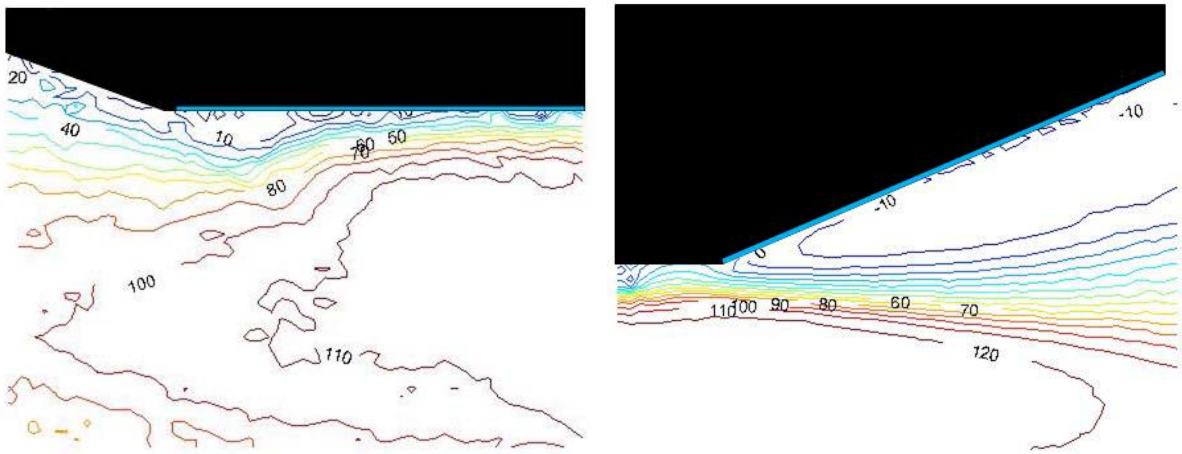

Figure 4: Streamwise velocity contours for the viewing angle of 90°, left plot, and 118°, right plot.

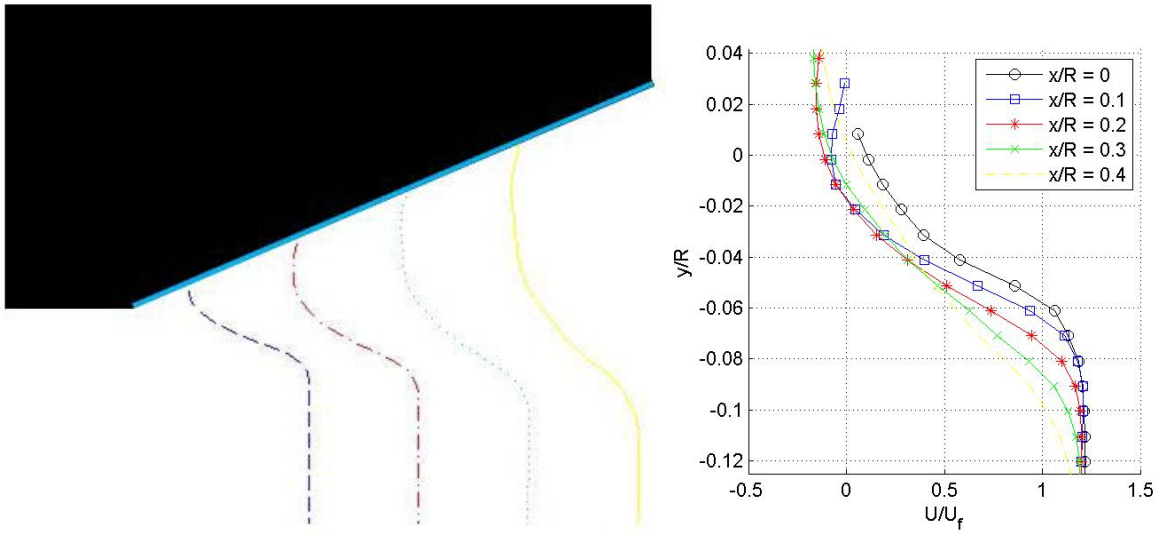

Figure 5: Velocity profiles for the viewing angle of 118°

Spatial distribution of aero-optical distortions

While velocity measurements were preformed along a center-plane only, inspection of the spatial distribution of aero-optical distortions over the aperture provided some information about spanwise effects on the wavefronts. Spatial distribution of the temporal wavefront variance, later simply called spatial distribution of OPDrms, shows spatial dependence of aero-optical distortions at different parts of the aperture. Spatial distribution of OPDrms for selected viewing angles for M = 0.3 and 0.4 are presented in Figures 6 and 7, respectively. At low viewing angles below 100 degrees spatial distribution revealed the presence of a compact region of elevated levels of aero-optical distortion near the center of the aperture for both M = 0.3 and 0.4 This region of higher aero-optical distortions is most probably due to the presence of the stationary unsteady vortical structure located on the aperture. This vortical structure is most likely formed as a shear from spanwise variation of the mean velocity field is stretched and intensified by an adverse pressure gradient over the aperture; it is similar in nature to "horn" vortices

observed forming on the back of the turret [1]. For larger viewing angles the separated flow over the aperture formed a spatially-growing shear layer with traveling vortical structures and resulted in the streamwise growth of the aero-optical distortions over the aperture. Some spanwise variations were still present in spatial distribution of OPDrms for large viewing angles, see Figures 6 and 7, suggesting the presence of the stationary vortical structure over the aperture.

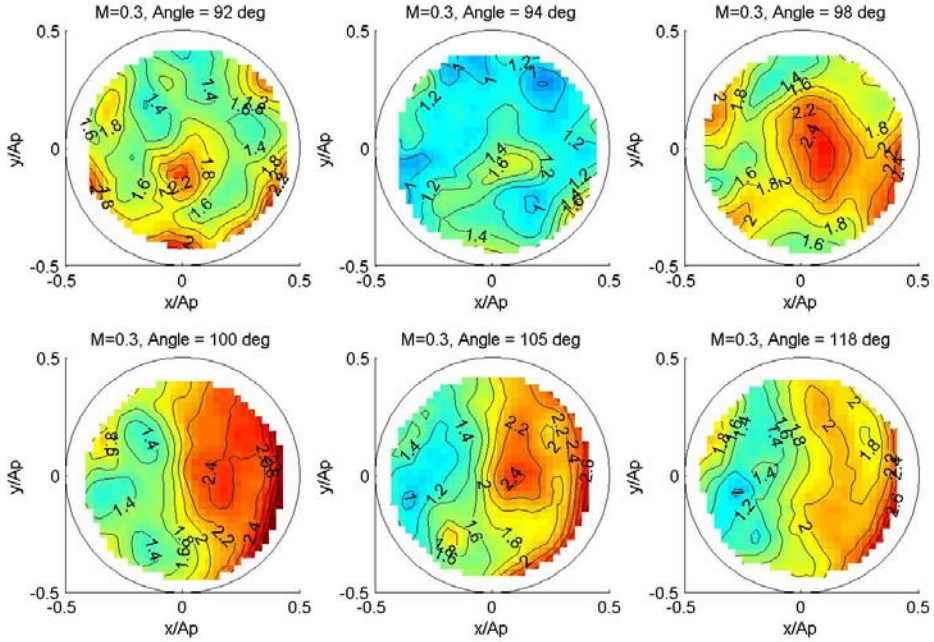

Figure 6: Spatial distribution of OPDrms at selected viewing angles, normalized by $(\rho/\rho_{SL})M^2D$. Incoming M = 0.3. Flow goes from left to right.

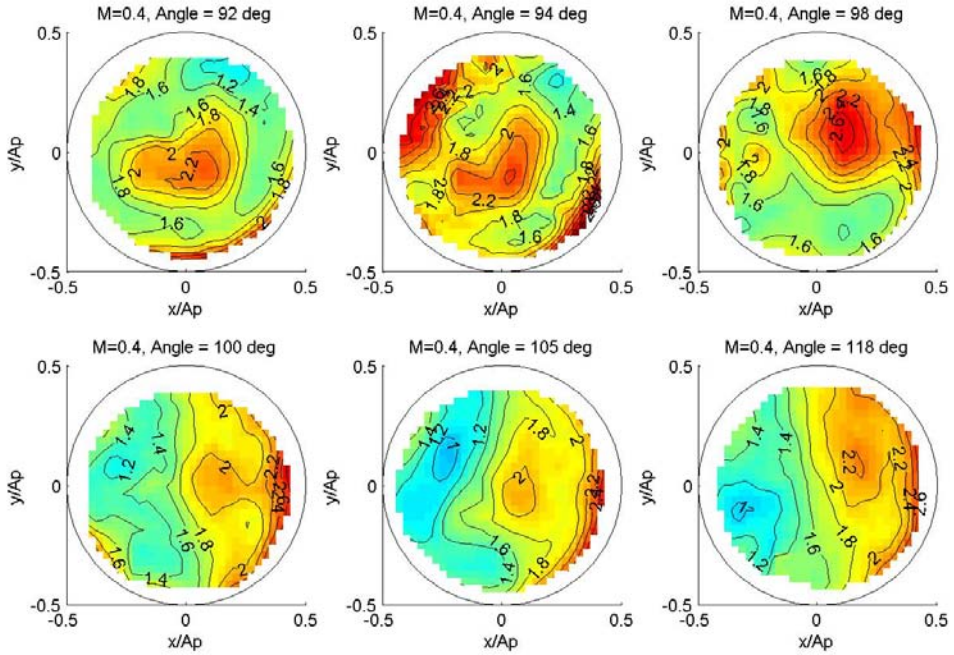

Figure 7: Spatial distribution of OPDrms at selected viewing angles, normalized by $(\rho/\rho_{SL})M^2D$. Incoming M = 0.4. Flow goes from left to right.

Local and global jitter

Jitter data were collected for viewing angles ranging from 90° to 118° at M = 0.3 and M = 0.4 and mechanically-induced jitter was removed from the total jitter using the LSE technique discussed earlier, so only the aero-optical jitter will be discussed in this paper. Figure 8 shows the evolution of the spectra of both the global and local jitter as the viewing angle changes for M = 0.3 and M = 0.4. The jitter spectra were normalized as $\hat{\theta}_{Norm}(f) = \hat{\theta}(f) / \left(\frac{\rho M^2 D}{\rho_{SL} U_\infty} \right)$, as suggested in [8]. The frequency was normalized as $St_D = fD/U_\infty$.

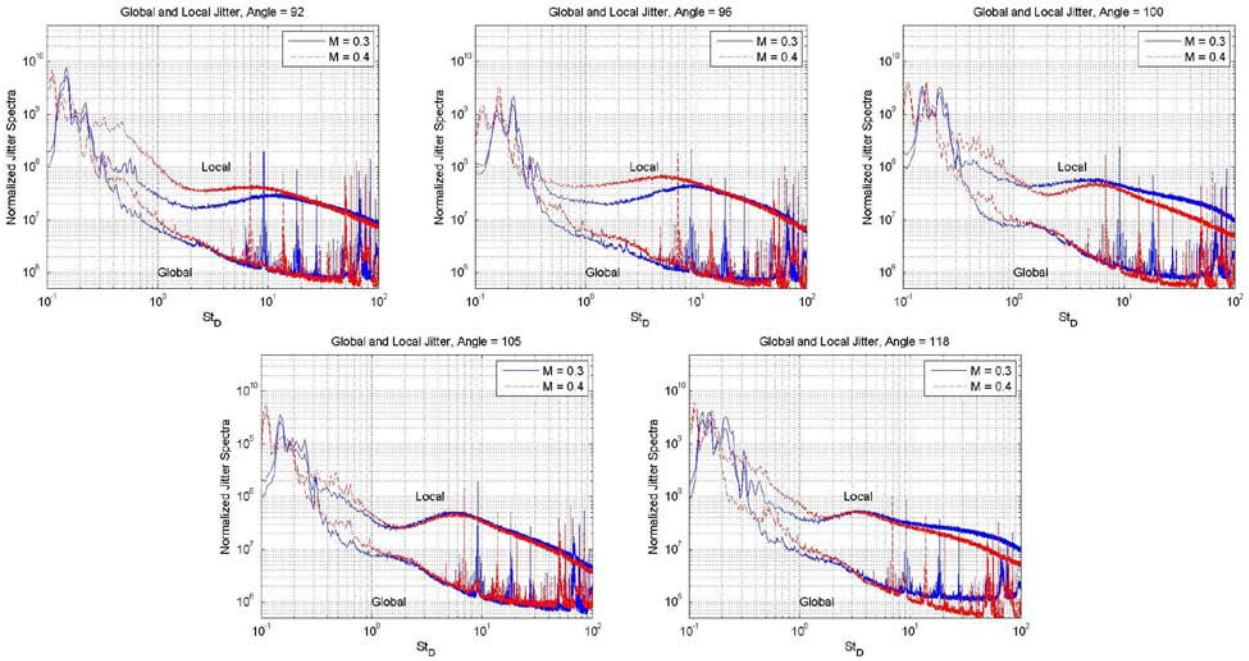

Figure 8: Spectra of global and local jitter for varying viewing angles.

At low frequencies $St_D < 0.4$ sharp peak in both the global and the local jitter is due to mechanical vibrations of the tunnel windows and/or vibration of optical components, which, unlike the mechanically-induced jitter due to the turret motion, were not be measured by accelerometers and therefore were not removed using the LSE technique. Above $St_D = 0.4$, the local jitter spectra had significantly more higher-frequency content compared to the global jitter spectra for all viewing angles and Mach numbers. Series of sharp peaks in the local jitter spectra are due to electronic noise. As it will be shown later in this paper, this is due to the finite size of the collimated laser beam, so-called aperture effects, which essentially works as a low-pass filter [9]. At the viewing angles of 92 and 96 degrees, the normalized global jitter does not exhibit the self-similar behavior, which can be contributed to transient effects in the flow at these angles; similar conclusions were made when analyzing the 2-D wavefront data earlier in this paper. For higher viewing angles above 100 degrees, the wavefronts were shown to be self-similar for different Mach numbers, and so were the observed global jitter spectra, although small deviations between normalized spectra were found for $0.4 < St_D < 1$.

The normalized local jitter spectra were also affected by the contaminating mechanical jitter due to the vibrating tunnel windows for $St_D < 0.4$. In the range of normalized frequencies between 0.4 and approximately 2, the local jitter spectra monotonically decreased, although at a slower rate that the global jitter spectra. Above $St_D = 2$, the local jitter spectra has a "hump"; the location of the hump depended on the viewing angle and, at small back-looking angles, depended also on the incoming Mach number. For angles of 92 and 96 degrees, the 'hump" is most probably due to the boundary layer formed over the flat window; the lack of collapse of the spectra at high frequencies is, again, due to the flow transient effects at small looking-back angles. For viewing angles above 100 degrees, this peak was identified with travelling aero-optical effects from vortical structures inside the shear layer over the aperture; the similar "hump" in spectra was observed in the separated, shear-layer-dominant region over the conformal-window turret [10]. The local jitter spectra were self-similar at different Mach numbers for large viewing angles, consistent the earlier conclusion from the analysis of the wavefront statistics that the flow and aero-optical distortions were self-similar at these angles.

When the shear-layer was formed over the aperture, the global jitter spectra were found to collapse for all viewing angles above 100 degrees, see Figure 9, while the local jitter spectra didn't show collapse at these viewing angles (not shown). In the next section it will be shown that the predominant source of the global jitter at low frequencies below $St_D = 1.5$ is a stationary aero-optical structure; traveling aero-optical distortions affect the global shear layer at higher frequencies. The self-similarity of the global jitter spectra for viewing angles above 100 degrees suggested a global source of stationary aero-optical distortions, which are largely independent of the local traveling vortical structures in the flow directly over the aperture. One of the possible sources of the stationary aero-optical distortions is global unsteady pressure fluctuations caused by the stationary necklace vortex near the bottom of the turret, as well as the slowly-varying recirculation region in the near wake downstream of the turret. This conclusion is partially supported, although indirectly, by unsteady pressure measurements performed in the near wake of the turret [10] showing that most of the pressure fluctuations in the necklace-vortex-dominated wake occur at low frequencies, $0.1 < St_D < 0.8$.

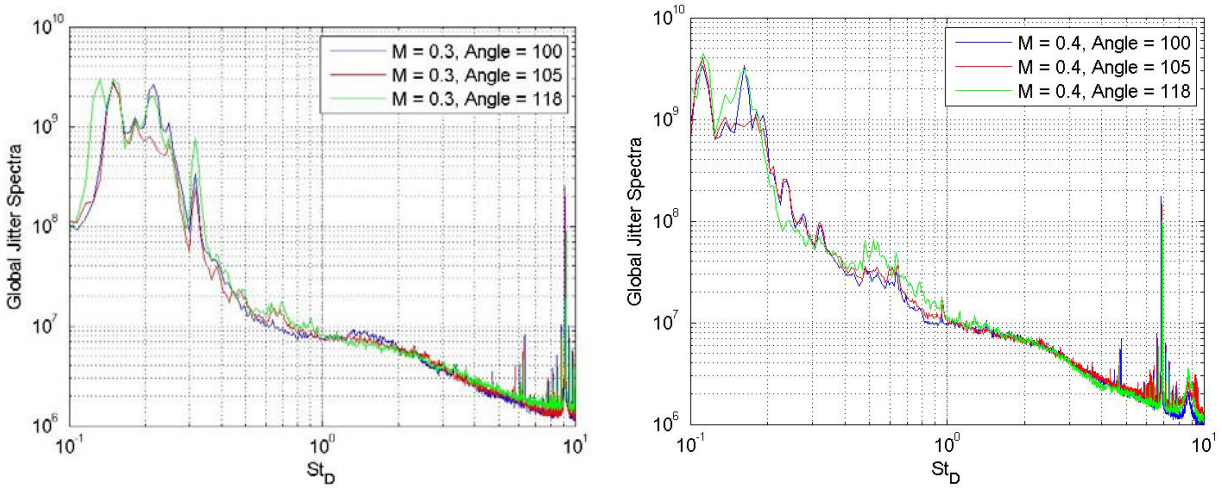

Figure 9: Normalized global jitter spectra for M=0.3 (left plot) and M=0.4 (right plot) for viewing angles of 100, 105 and 118 degrees.

Correlation between local and global jitter

Plots of the normalized spectral correlation, both the amplitude and the phase, between the global and the local jitter as a function of the normalized frequency, St_D, are presented in Figure 10 for 92 and 98 degrees for two Mach numbers. Spectra of the global and the local jitter are also plotted in Figure 10. The local jitter was measured approximately 17 mm upstream of the center of the aperture and, as it will be shown later in this paper, parts of the phase plot with a zero phase between the local and the global jitter indicate the presence of the stationary aero-optical structure, while frequency ranges with the linearly-changing phase is indicative of the traveling wavefront. For the viewing angle of 92 degrees effects of the stationary aero-optical aberrations are present at low range of frequencies $St_D < 2.5$, as the phase is zero in this range For larger frequencies $3 < St_D < 7$, aero-optical distortions have a weak traveling component, most probably from the perturbed boundary layer over the aperture. It is worth noting that the local jitter spectrum has a local minimum at $St_D \sim 2.5$, 'dividing' the spectrum into a part dominated by the stationary-structure at low frequencies $St_D < 2.5$ and a traveling-structure-dominant component at higher frequencies $St_D > 2.5$. Correlation levels are stronger for M = 0.4 for the stationary-structure frequency range, again indicating possible transient Re-number effects at this viewing angle. A similar pattern can be observed for the viewing angle of 98 degrees, although the frequency range of the stationary-dominant effects is at a narrower range of $St_D < 1$. A lack of collapse in global and local jitter spectra and in normalized correlation values for M = 0.3 and 0.4 also point toward transient Re-number effects at this angle. Finally, low values of correlation between the global and the local jitter and significant amount of scatter in phase suggest a relatively weak stationary aero-optical effects or large amount of incoherent aero-optical distortions.

After the shear layer was formed over the aperture for large viewing angles of 100 degrees and above, both the amplitudes and the phases of the correlation collapse for both Mach numbers, indicating the self-similarity of the underlying aero-optical distortions. The correlation is nearly one for very small frequencies, where corrupting mechanically-induced effects are present on both the global and the local jitter. Aero-optical distortions are stationary in nature for St_D between 0.4 and approximately 1.5, as suggested by the zero-phase correlation between the global and the local jitter, with correlation levels around 0.3. Around $St_D = 1.5$, the correlation levels drop, while

the phase shifts to positive levels. For higher frequencies between $1.5 < St_D < 6$, the correlation amplitude goes back to 0.3 and the phase has a negative slope, indicating the presence of the travelling aero-optical structure. Above $St_D = 6$, the local and the global jitter become largely uncorrelated.

Note that, the amplitude of correlation between the global and the local jitter remained around 0.3 for viewing angles between 100 and 118 degrees, except for a drop in correlation values around $St_D = 3.5$, as seen in Figure 11; the stronger is the shear layer, the larger is the drop, see Figure 11, right. From Figure 11 it follows that the location of the drop is independent of the Mach number. Moreover, the phase of the correlation has a larger negative slope crossing a zero at the same value of $St_D = 3.5$. This effect was contributed to aperture effects and it will be considered in the next section.

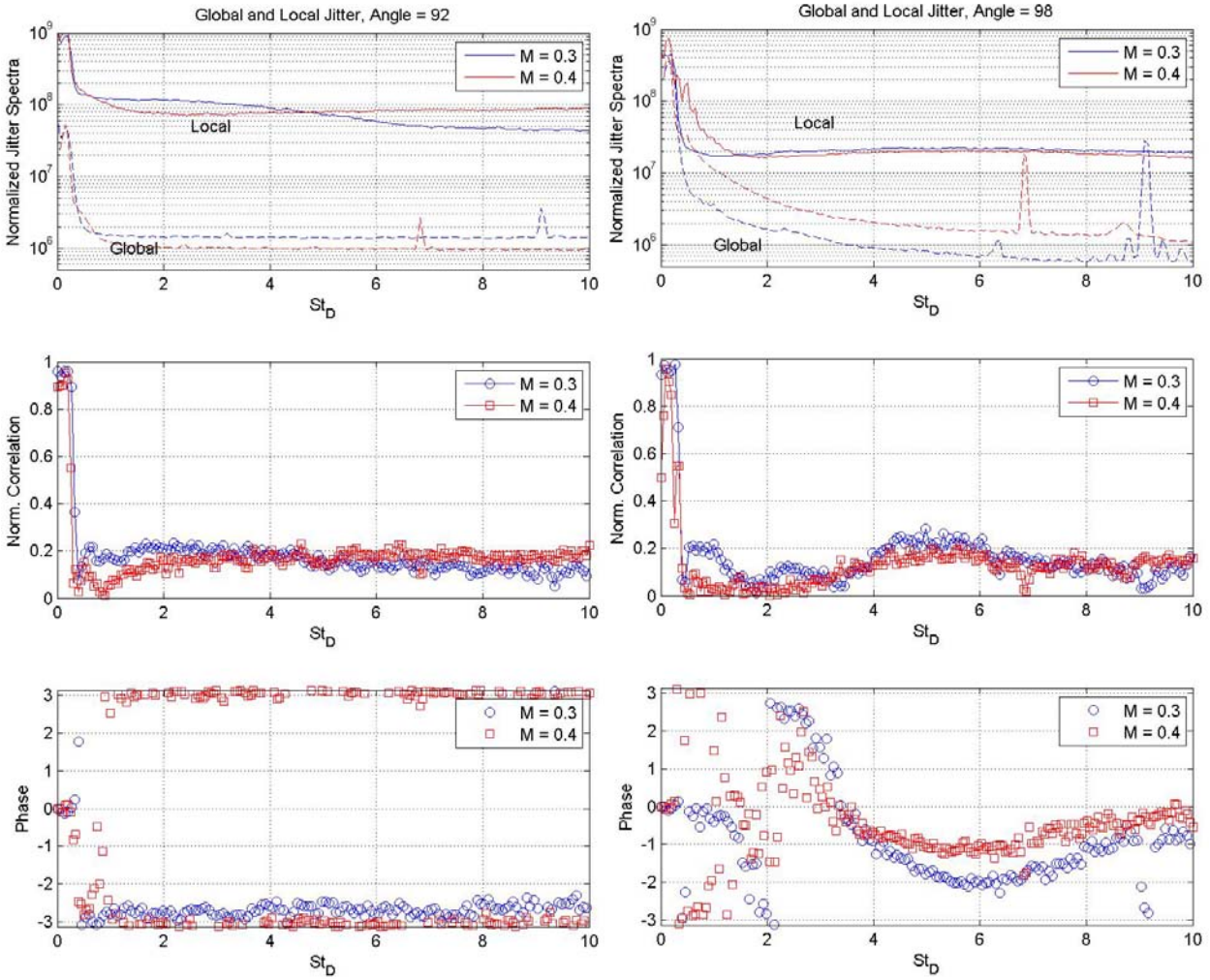

Figure 10: Spectra of the global and local jitter (top plots), amplitude (middle plots) and phase (bottom plots) of the normalized spectral correlation between the global and the local jitter for viewing angle of 92 degree (left plots) and 98 degrees (right plots).

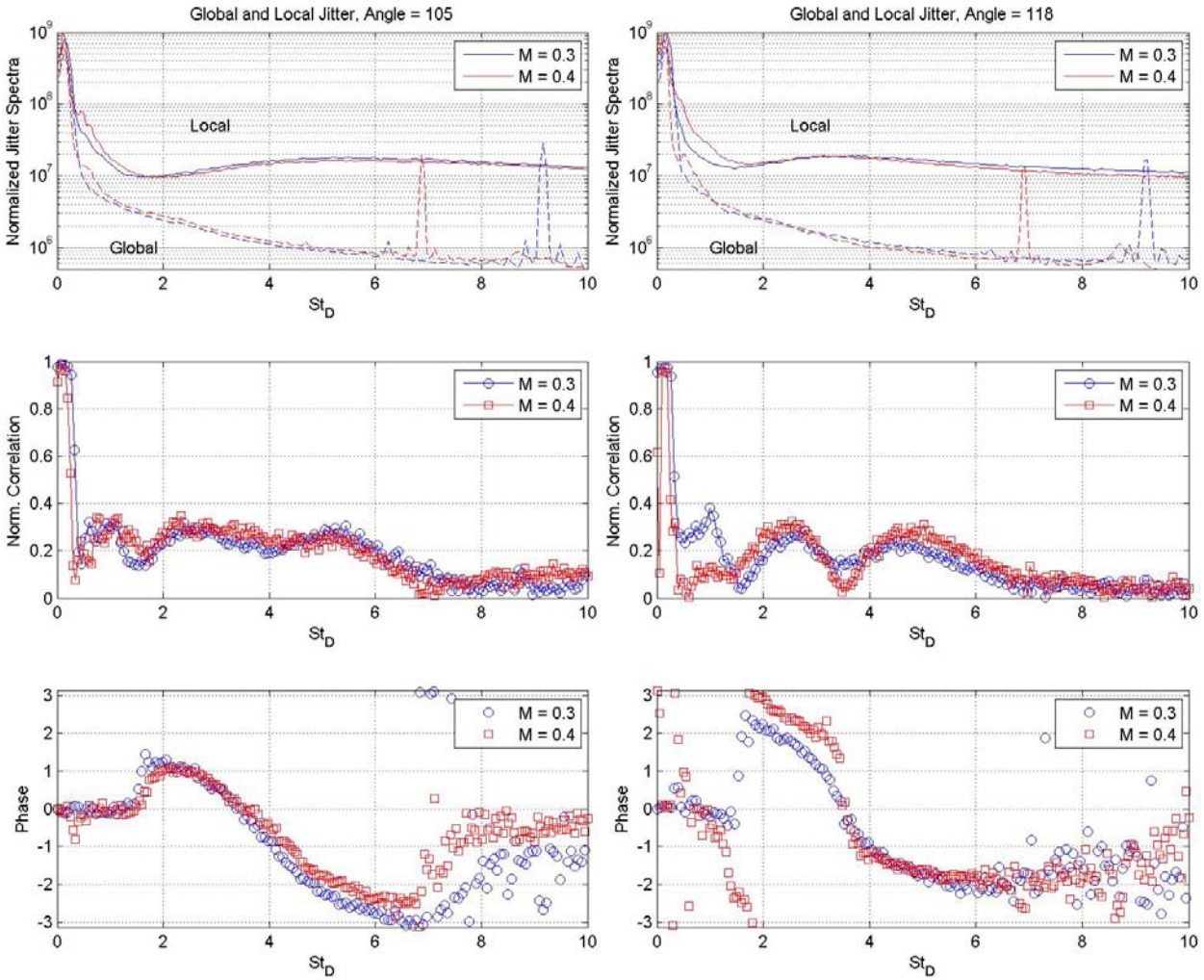

Figure 11: Spectra of the global and local jitter (top plots),absolute value (middle plots) and phase (bottom plots) of the normalized spectral correlation between the global and the local jitter for viewing angle of 105 degree (left plots) and 118 degrees (right plots).

Aperture effects on global jitter

To explain the drop in correlation amplitude and the change in the phase slope around St_D = 3.5 for viewing angles larger than 100 degrees, let us recall the relation between the global and the local jitter. As the local jitter at these angles was shown to be dominant by the traveling shear-layer aero-optical structures at frequencies greater than St_D = 2, consider for simplicity a pure harmonic one-dimensional traveling wavefront, $W(x,t) = \sin\left(k_x(x - U_C t)\right)$. The local jitter at a fixed point is simply a negative spatial derivative of the wavefront, $\theta(x,t) = -k_x \cos\left(k_x(x - U_C t)\right)$. The global jitter or tip/tilt depends not only on the wavefront but also on the size of the aperture, *Ap*, as it is a (negative) linear fit to an *apertured* wavefront. In [9] it was shown that the global jitter can be calculated from the apertured wavefront as $A(t) = -\int_{-Ap/2}^{Ap/2} W(x,t)\,x\,dx \Big/ \int_{-Ap/2}^{Ap/2} x^2\,dx$. Performing the integration for the pure harmonic wavefront, the global jitter can be found as, $A(t) = -k_x \cos(2\pi f t)\cdot G_A(z = Ap/\Lambda)$, where $G_A(z) = 3\left[\sin(\pi z) - \pi z\cos(\pi z)\right]/(\pi z)^3$ is the aperture-dependent transfer function and $\Lambda = 2\pi/k_x$ is the wavefront spatial wavelength. The plot of $G_A(z)$ is presented in Figure 12, left plot. For large wavelengths, *z* is small and the wavefront can be faithfully represented by a linear component only, as seen in Figure 12, top right plot. As a consequence, the G_A-function is close to one for small *z*. However, for wavelengths comparable with or smaller then the aperture size, the wavefront varies significantly over the aperture and the linear fit does a poor job representing

the wavefront, see Figure 12, bottom right plot, leading to small values of G_A-function. Moreover, for some wavelengths, for instance, for $1.43 < Ap/\Lambda < 2.46$, the G_A-function becomes negative, meaning that the global jitter is *out-of-phase* with the local jitter.

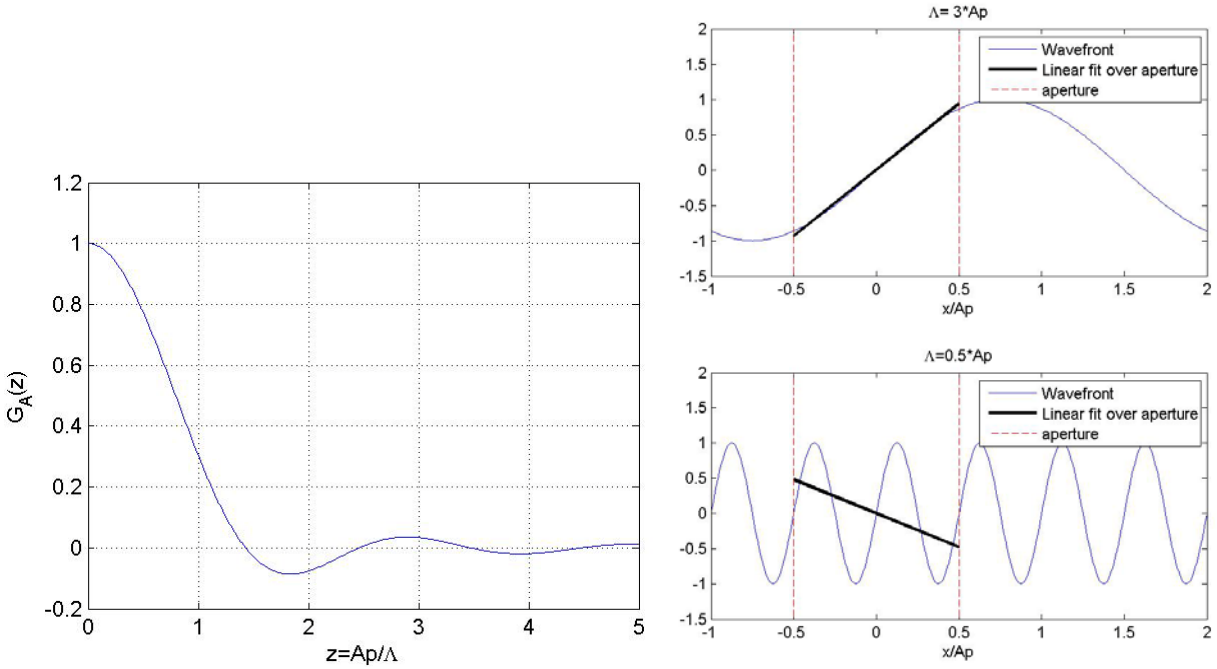

Figure 12: Left: G_A as a function of aperture size and wavelength. Right: Examples of the wavefronts and the global tip/tilt over the aperture for Wavelength/Apeture ratios of 3 and 0.5.

Recall that the local jitter was measured at the location Δ = -17 mm apstream of the center of the apetrure. Thus, the local jitter in this location becomes $\theta(x=\Delta,t)=-k_x\cos\left(k_x(\Delta-U_C t)\right)=-k_x\cos\left(2\pi f(\Delta/U_C-t)\right)$, thus advancing the global jitter $A(t)=-k_x\cos(2\pi ft)\cdot G_A(z=Ap/\Lambda)$ by a fixed time, $\tau = \Delta/U_C$. It is easy to show [3] that in the frequency domain, the phase slope between the global and the advanced local jitter will be $dArg[S(f)]/df = 2\pi\tau = 2\pi\Delta/U_C$. When the wavefront wavelength approaches Λ = 1.43Ap, the global jitter becomes zero and for smaller wavelengths, the G_A-function becomes negative, resulting in the π-jump in the correlation phase at Λ = 1.43Ap. Replacing the spatial wavelength with frequency, the location of the π-jump in phase in St_D-space will be $1.43(D/Ap)(U_C/U_\infty)$. From Figure 11, the location of the zero-correlation and the zero-phase-crossing is at approximately St_D = 3.5. Since D/Ap = 3, from here it follows that the convective speed of the traveling optical structure is $U_C/U_\infty = 3.5/1.43/3 = 0.81$, which is in very good agreement with direct measurements of convective speeds of 0.8 of the freestream reported in [5] at similar viewing angles and Mach numbers. Thus, for a pure traveling wavefront, the aperture effect on the global jitter causes the amplitude of the global jitter to drop to zero and the phase between the local and the global jitter to experience a π-jump.

In reality, in addition to the traveling component, the aero-optical distortions will have a stationary component and incoherent component. To see how they will affect the global-local jitter correlation, a simulated local jitter spectra was built, combining the stationary component at low frequencies, a time-advanced traveling component at high frequencies and incoherent, noise-like component as, $\hat{\theta}(f)=\hat{\theta}_{Stationary}(f)+\hat{\theta}_{Traveling}(f)e^{-2\pi if\tau}+\hat{e}(f)$. The global jitter spectrum becomes $\hat{A}(f)=\hat{A}_{Stationary}(f)+G_A(f)A_{Traveling}(f)+\hat{e}(f)$. The spectral correlation becomes, assuming the stationary and the traveling spectra are un-correlated, $S(f)=\dfrac{P_{Stationary}(f)+G_A(f)P_{traveling}(f)e^{2\pi if\Delta/U_C}}{\sqrt{|\theta(f)|^2|A(f)|^2}}$, where P(*f*) is the power spectrum.

Power spectra for simulated stationary and traveling components are shown in Figure 13, upper plot. Two cases, a "weak" and a "strong" traveling component were considered, in an attempt to simulate the shear layer with different strengths. Results of the simulated correlation amplitude and the phase for both cases are plotted in Figure 4, middle and bottom plots. Simulated results are in very good agreement with experimental values observed in Figure 11, with drops in the correlation value around 2 and 3.5, the phase zero-crossing near St_D = 3.5 and the increased phase slope for the "strong" traveling component.

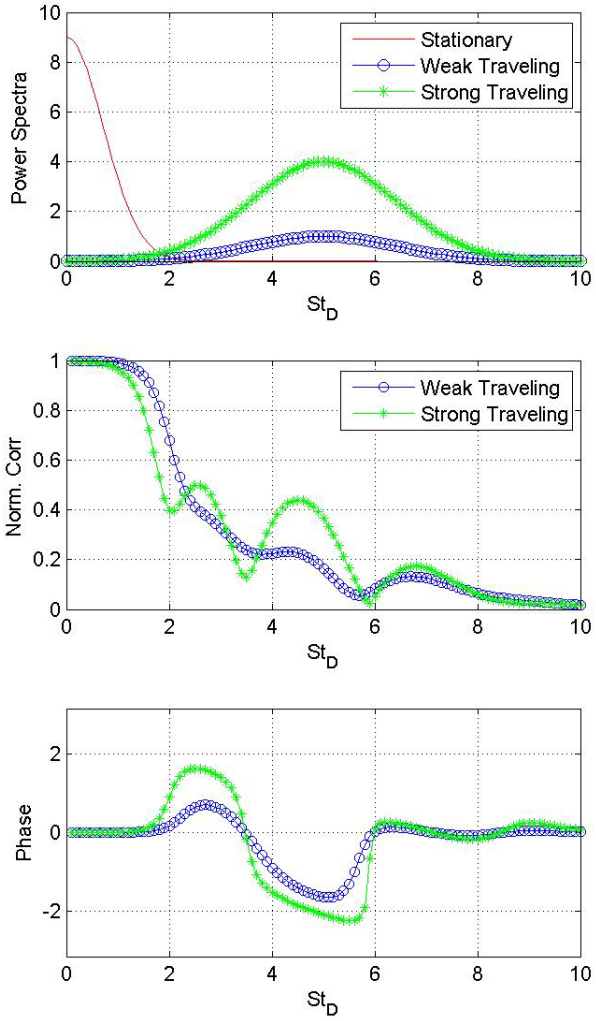

Figure 13: Different spectra components (top), normalized correlation amplitude (middle) and phase (bottom) plots between the local and the global jitter for a simulated wavefront, containing steady, traveling and incoherent components.

V. Conclusions

Extensive measurements of aero-optical environment around the flat-window turret over a range of looking-back angles were performed in order to identify sources of aero-optical distortions and their effect of the global jitter and higher-order wavefront components. Aero-optical measurements were performed simultaneously with accelerometers mounted inside the turret. Cross-correlating the mechanical motion of the turret with the measured jitter, both the global and the local jitter, allows one to separate the overall jitter into the mechanically-induced and the aero-optical components.

Wavefront measurements with complimentary velocity measurements revealed that in the range of viewing angles between 90 and 100 degrees, the flow over the flat-aperture has a small separation bubble immediately downstream of the leading slope discontinuity between the turret surface and the flat aperture, with the flow re-attaching over the main portion of the aperture. Details of the flow were found to be sensitive to the incoming Mach number. For larger viewing angles above 100 degrees, the separation bubble becomes an open separation region

with a spatially-growing shear layer over the flat-aperture; properly normalized aero-optical distortions were found to be independent of the incoming Mach number.

Normalized spectra of the global and the local jitter were also found to be weakly dependent on the incoming Mach number for the range of viewing angles between 90 and 100 degrees, and showed a self-similar behavior for larger viewing angles above 100 degrees. In addition, the global jitter was self-similar with Mach numbers for large viewing angles above 100 degrees, when the shear layer was present over the aperture. Studies of the amplitude and the phase of the cross-correlation between the global and the local jitter revealed that both the global and the local jitter are dominated by a stationary aero-optical structure at low frequencies $St_D < 1.5$, while the local jitter has an additional traveling component at higher frequencies $St_D > 2$. The stationary aero-optical structure is believed to be related to a global variation of the unsteady pressure field around the turret due to the low-frequency motion of the necklace vortex and the near wake. The traveling component was associated with the convecting vortical structures inside the shear layer. Aperture effects related to a finite size of the laser beam were experimentally observed and a simple model was successfully built to explain them.

Future work will further address important questions about the origin and dynamics of the stationary aero-optical structure by simultaneously measuring unsteady pressure near the bottom of the turret and in the near wake and velocity field around the turret and cross-correlating it with the global jitter over a wide range of the forward- and back-looking viewing angles.

References

[1] S. Gordeyev and E. Jumper, “Fluid Dynamics and Aero-Optics of Turrets”, *Progress in Aerospace Sciences*, **46**, (2010), pp. 388-400.

[2] Gilbert, K. G. and Otten L. J. (eds), “Aero-Optical Phenomena,” Progress in Astronautics and Aeronautics, Vol. 80, pp. 1-9, AIAA, New York, 1982.

[3] S. Gordeyev, J.A. Cress, E. Jumper and A.B. Cain, "Aero -Optical Environment Around a Cylindrical Turret with a Flat Window", *AIAA Journal*, Vol. **49**, No. 2, pp. 308-315, 2011.

[4] Z. Ponder, S. Gordeyev, E. Jumper, S. Griffin, C. McGaha, “Passive Mitigation of Aero-Induced Mechanical Jitter of Flat-Windowed Turrets”, AIAA Plasma Dynamics and Lasers, 2011.

[5] S. Gordeyev, T. Hayden and E. Jumper, "Aero-Optical and Flow Measurements Over a Flat-Windowed Turret", *AIAA Journal*, vol. 45, No. 2, pp. 347-357, 2007.

[6] Adrian, R.J., “On the role of conditional averages in turbulent theory”, In: Turbulence in Liquids: Proceedings of the 4th Biennial Symposium on Turbulence in Liquids, ed. G. Patteson and J. Zakin, Science Press, Princeton, 1977, pp. 322-33

[7] C. Porter, S.Gordeyev, M. Zenk and E. Jumper, ”Flight Measurements of Aero-Optical Distortions from a Flat-Windowed Turret on the Airborne Aero-Optics Laboratory (AAOL)”, AIAA Paper 2011-3280.

[8] D. Wittich, S. Gordeyev and E. Jumper, "Revised Scaling of Optical Distortions Caused by Compressible, Subsonic Turbulent Boundary Layers”, AIAA Paper 2007-4009.

[9] John P. Siegenthaler, “Guidelines for Adaptive-Optic Correction Based on Aperture Filtration”, Ph.D. Thesis, University of Notre Dame, 2008.

[10] S. Gordeyev, M. Post, T. MacLaughlin, J. Ceniceros and E. Jumper, "Aero-Optical Environment Around a Conformal-Window Turret", *AIAA Journal*, vol. 45, No. 7, pp. 1514-1524, 2007.